Supplementary Information (SI) for Nanoscale Horizons.
This journal is © The Royal Society of Chemistry 2026

Supporting Information for:

# Ferroelectricity in Wurtzite Atomic Layer Annealed Aluminum Nitride Thin Films

Dominic A. Dalba,[a] Dilan M. Gamachchi,[a] Indeewari M. Karunarathne,[a] Bipin Bhattarai,[a] Xiaoman Zhang,[b] Wangwang Xu,[c] Somayeh Saadat Niavol,[a] Dongmei Cao,[c] W.J. Meng,[c] Andrew C. Meng[a*]

[a] Department of Physics and Astronomy, University of Missouri, Columbia
[b] Department of Engineering and Industrial Professions, University of North Alabama
[c] Department of Mechanical and Industrial Engineering, Louisiana State University
* Corresponding author email: acmeng@missouri.edu

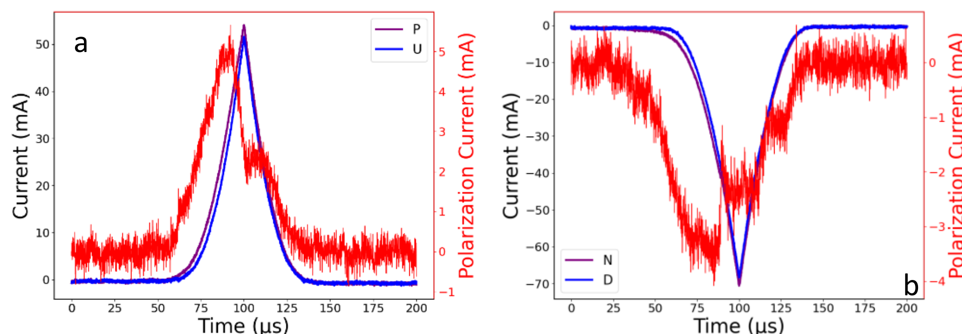


Fig. S1. Raw a) P, U; b) N, and D current transients plotted on identical axes. Polarization currents a) P – U and b) N – D are shown in red

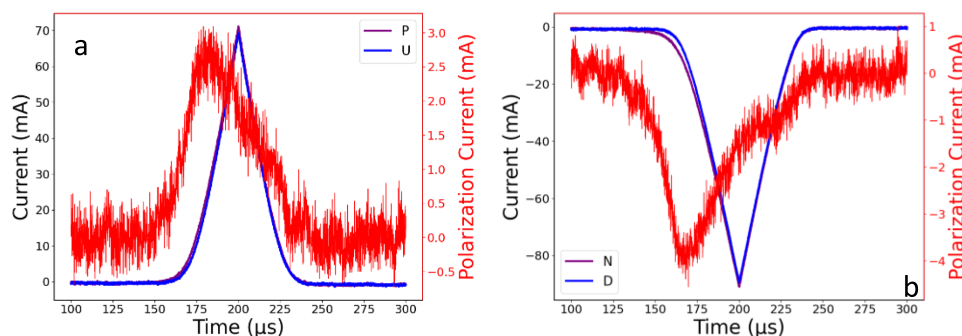


Fig. S2. Raw a) P, U; b) N, and D current transients plotted on identical axes. Polarization currents a) P – U and b) N – D are shown in red

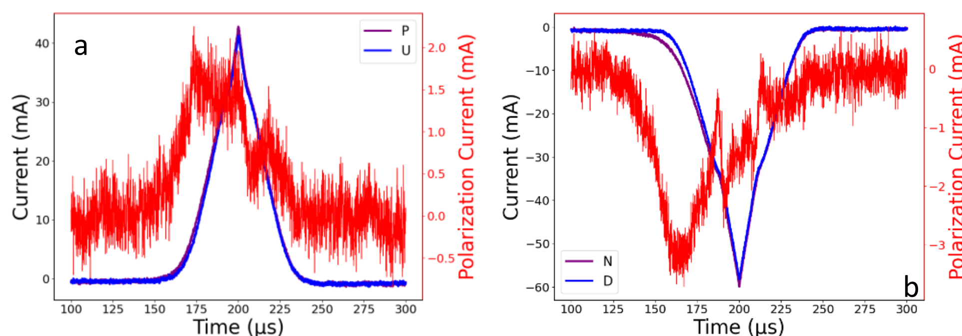


Fig. S3. Raw a) P, U; b) N, and D current transients plotted on identical axes. Polarization currents a) P – U and b) N – D are shown in red

| Delay Time (s) | $P_r$ (μC cm$^{-2}$) @ 36V |
|---|---|
| $5 \times 10^{-4}$ | 31.9 ± 1.3 |
| $1 \times 10^{-4}$ | 32.7 ± 2.6 |
| $1 \times 10^{-5}$ | 30.0 ± 4.5 |

Table S1. Effect of varying delay time on $P_r$ (pulse width = $2 \times 10^{-7}$ s, rise/fall time = $10^{-4}$ s)

| Pulse Width (s) | $P_r$ (μC cm$^{-2}$) @ 36V |
|---|---|
| $2 \times 10^{-7}$ | 32.7 ± 2.6 |
| $5 \times 10^{-5}$ | 37.2 ± 2.8 |
| $1 \times 10^{-5}$ | 66 ± 16 |

Table S2a. Effect of varying pulse width on $P_r$ (delay time = $1 \times 10^{-4}$ s, rise/fall time = $10^{-4}$ s)

| Pulse Width (s) | Corrected $P_r$ (μC cm$^{-2}$) @ 36V |
|---|---|
| $2 \times 10^{-7}$ | 32.7 ± 2.6 |
| $5 \times 10^{-5}$ | 32.8 ± 3.4 |
| $1 \times 10^{-5}$ | 28.5 ± 4.8 |

Table S2b. Effect of varying pulse width on $P_r$ (delay time = $1 \times 10^{-4}$ s, rise/fall time = $10^{-4}$ s) with additional polarization current during constant voltage part of pulse (assumed to be polarization dependent leakage) subtracted

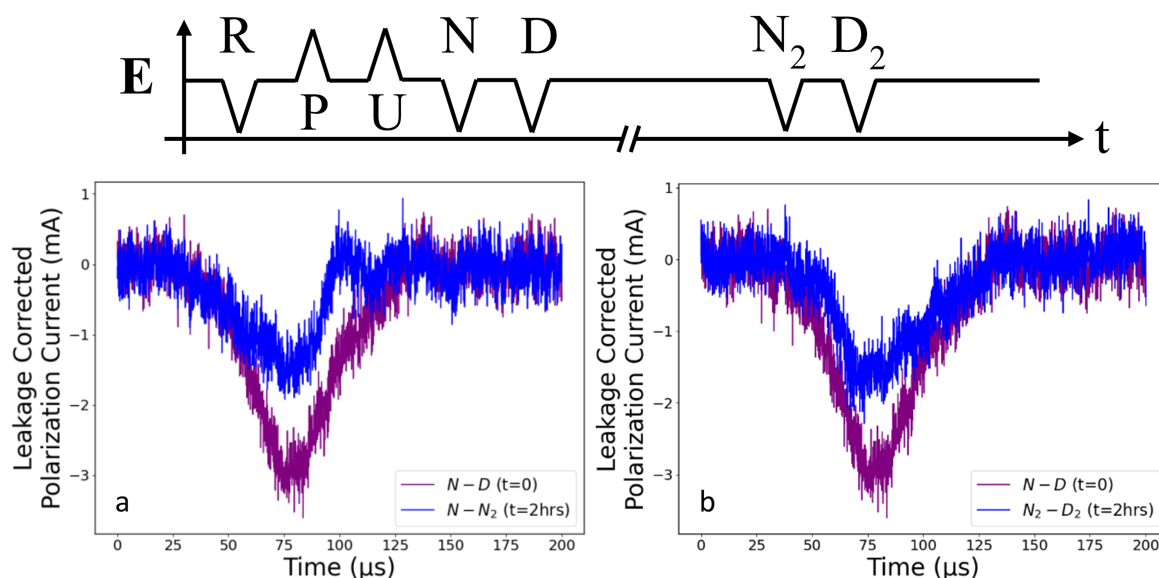


Fig. S4. Change in leakage corrected polarization current (N – D) vs. (N – $N_2$) and ($N_2$ – $D_2$) showing decay consistent with depolarization induced loss of retention

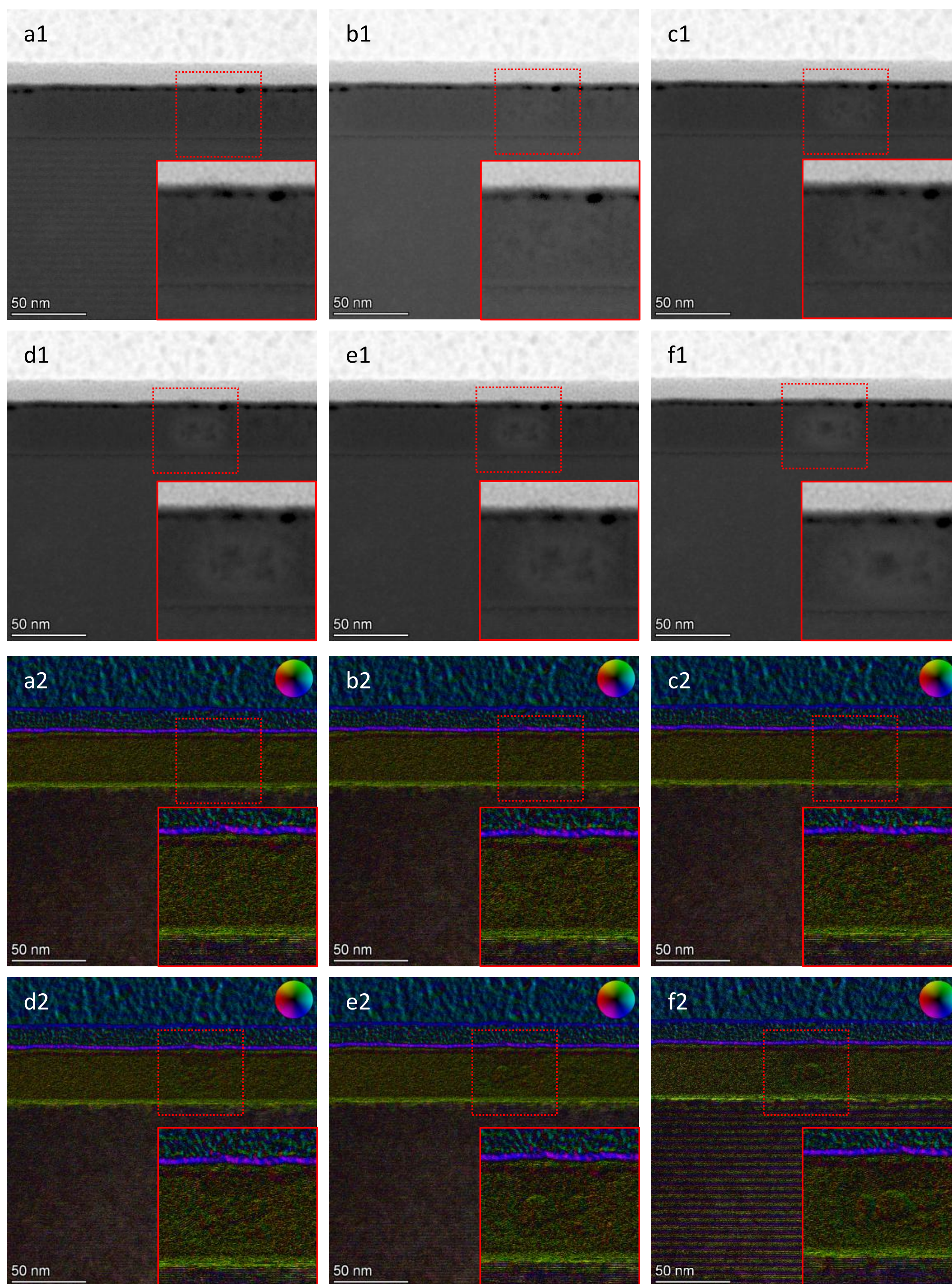


Fig. S5. Time lapse HAADF STEM (1) and STEM-DPC (2) images of ALA AlN as a function of successively higher electron beam dose from (b – f) using reduced raster scanning in the red dotted rectangle area: (a) pristine, (b) a + 50 frames (10 µs), (c) b + 50 frames (20 µs), (d) c + 50 frames (20 µs), (e) d + 50 frames (20 µs), (f) e + 50 frames (20 µs). Beam current is ~ 100 pA and dwell time is given in the parentheses.

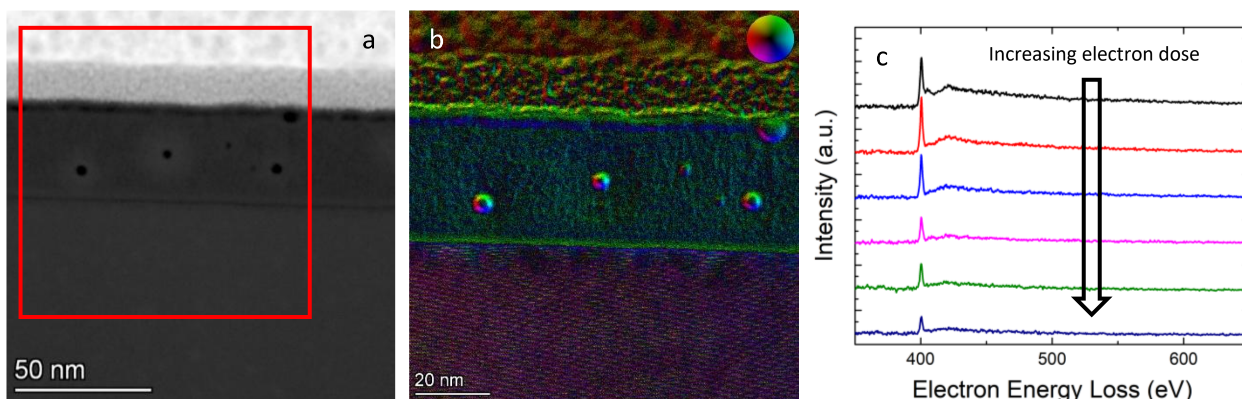


Fig. S6. a) HAADF STEM image of AlN with holes generated by electron beam irradiation; b) corresponding STEM-DPC image showing electric field modulation at holes; c) EELS spectrum time series at a single point showing evolution of N-K edge (decrease in intensity) as electron beam irradiation generates a hole

Electron Energy Loss Spectroscopy (EELS) in STEM was measured using the Gatan EF-CCD camera in Dual EELS mode at a 37 mm camera length using a 5 mm Gatan imaging filter (GIF) aperture to yield a collection angle of 100 mrad.

We have characterized point defects in ALA AlN intentionally generated through electron beam exposure in the TEM. Figures S5a-f show sequential time series HAADF STEM and STEM DPC imaging in which a reduced raster window inside the dotted rectangle is scanned 50 times between images. Figure S5a shows pristine AlN; while the changes in contrast in Figures S5b-c are less obvious, the magnified insets of the region in the dotted rectangle in Figures S5d-f clearly show a growing bubble shaped feature circled in red in the insets.

Figure S6a shows a high angle annular dark field (HAADF) STEM image with several electron beam induced holes – these resulted from long beam dwell times from collecting EELS spectra time series (Fig. S6c). The EELS spectrum time series was collected at a frame acquisition rate of 0.05s per frame – the spectra (Fig. S6c) show integrations of frames 1-5 (black trace), 6-10 (red trace), 11-15 (blue trace), 21-25 (magenta trace), 31-35 (green trace), and 41-45 (navy trace). The initial EELS spectrum (black trace) corresponds to a point defect concentration close to that of the bulk crystal, and the point defect concentration in the AlN film increases in each successive EELS spectrum (Fig. S6c). We can see that the N-K edge has a small shoulder in the first spectrum, but that this feature decreases as a function of increasing electron dose. To rationalize this observation, we consider that the electron beam has a finite size: thus, when a hole is first generated, electrons hit an annular region around the hole in which the local coordination of atoms is slightly decreased (i.e. there is a local increase in vacancy concentration). Figure 6b shows a STEM DPC image showing contrast consistent with local electric field modulation at the electron beam induced holes. This may occur due to an imbalance in stoichiometry, which would result in a cluster of either Al or N vacancies near the hole. We also observe that lower concentrations of point defects are also visible in STEM DPC imaging, although the contrast is not as pronounced.

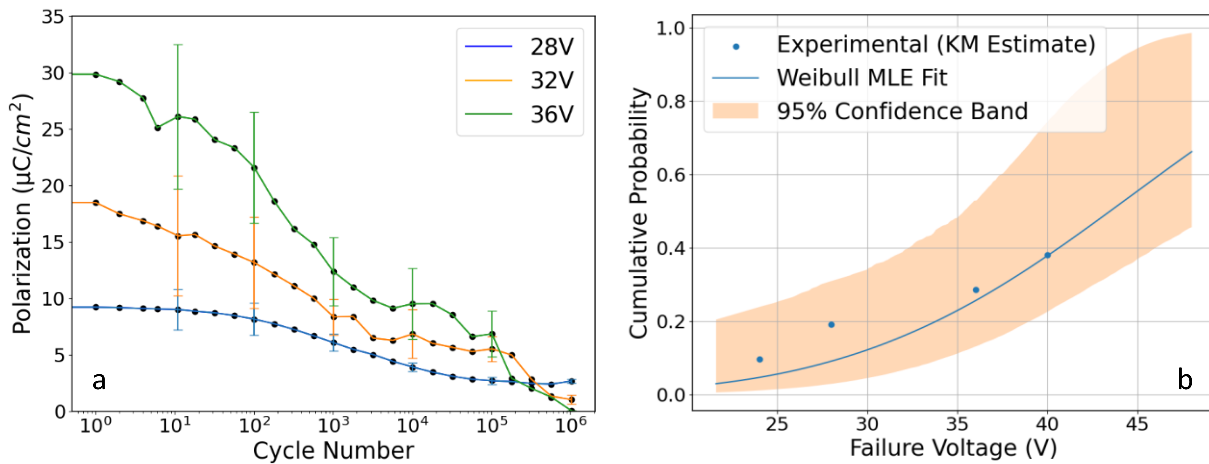


Fig. S7. a) Endurance cycling of ALA wurtzite AlN ferroelectric capacitors; b) fit of cumulative device failure probability to Weibull cumulative distribution

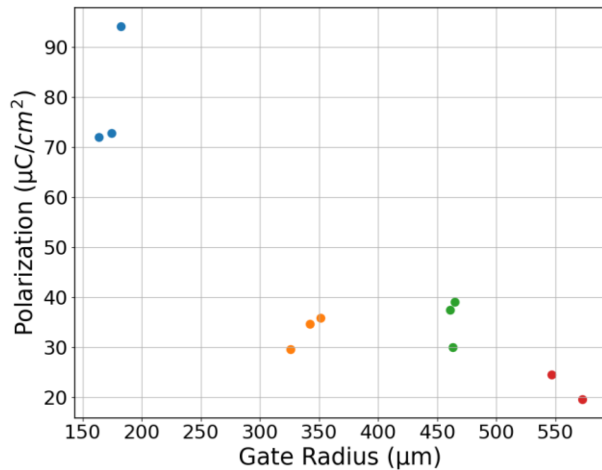


Fig. S8. Gate size dependence of polarization

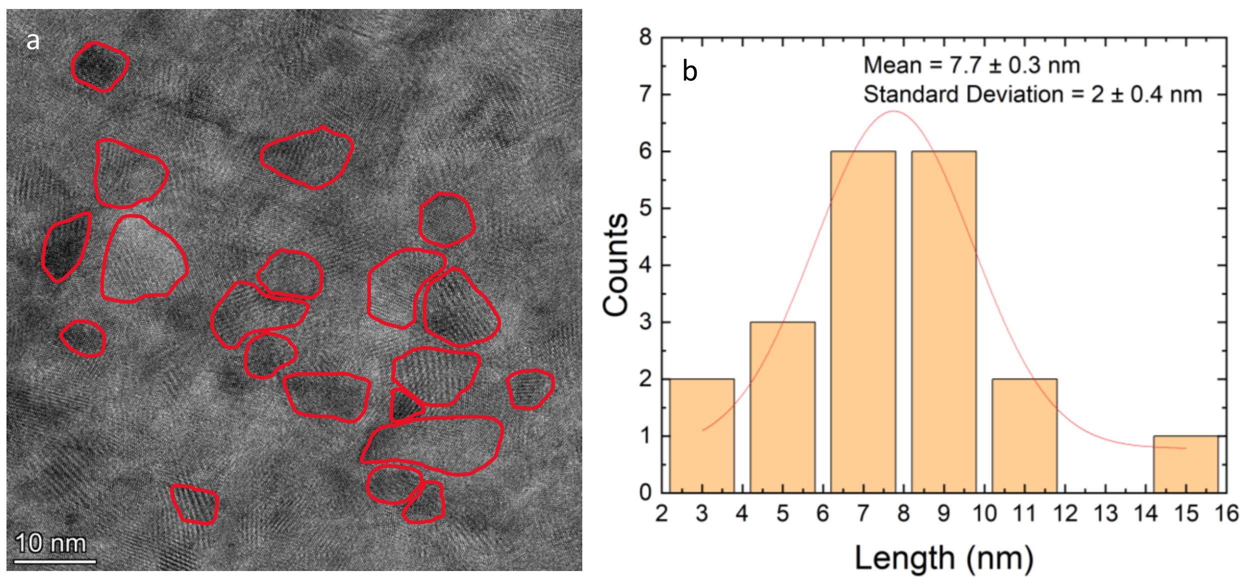


Fig. S9. a) Grains segmented by Moiré contrast in plan-view HRTEM image; b) grain size distribution